Internal Transport Barriers time evolution in QSH discharges

A .Alfier, A.Fassina, P. Franz, M. Gobbin, B.Momo, A.Ruzzon

Consorzio RFX, Euratom/ENEA Association, Padova, Italy

1) Background and Tools

In the last years, a new paradigm for the reversed field pinch (RFP) equilibrium has been developed, in which the equilibrium fields are driven by a single magnetic eigenmode (QSH-Quasi Single Helicity state[1]). This state is characterized by the suppression of magnetic chaos and associated particle and energy transport, with the development of an internal transport barrier (ITB). In this work, we will analyze the thermal and transport features of the QSH states. In particular, the analysis of heat transport as a function of the magnetic spectrum is required to understand the performance and limits of the QSH.

The electron temperature (T_e) profiles commonly used in confinement studies are obtained - in the RFX-mod machine – with the Thomson Scattering (TS [2]) diagnostic, which provides high spatial resolution, and is capable of a maximum repetition rate of 50 Hz. The present work uses the multichord double filter SXR spectrometer (DSXC [3]) to complement the TS profiles with a higher time resolution (up to 5 kHz), in order to get a more complete database to compare with the magnetic spectra. The advantage is in the study of the dynamics of QSH cycles in a single discharge with respect to the more heterogeneous data coming from the TS diagnostic in different discharges. The obvious disadvantage lies in the poorer spatial resolution of the DSXC with respect to the TS; moreover, the TS measures are punctual, while DSXC gives line-integrated temperature measurements.

The DSXC diagnostic consists of ten lines of sight, with impact parameter varying from r/a=0 to r/a=0.8: the plasma bremsstrahlung spectrum ($S(E) \propto T^2 e^{-T/h\nu}$) is sampled with two energy cutoffs thanks to ten couples of beryllium filters, each couple (one chord) consisting of elements of different thickness. The diagnostic returns the maximum T_e value along each line of sight; the latter is evaluated considering, in the x-ray emissivity model, standard temperature and density profiles.

The first step of the analysis is to understand the limits of the DSXC diagnostic in the gradients evaluation, in particular as far as the growth of a hot, localized structure is concerned. The shape of QSH T_e profiles differ from the standard ones, used in the simulation for temperature reconstruction; for this reason, DSXC data could be affected by a systematic deviation with respect to real T_e values.

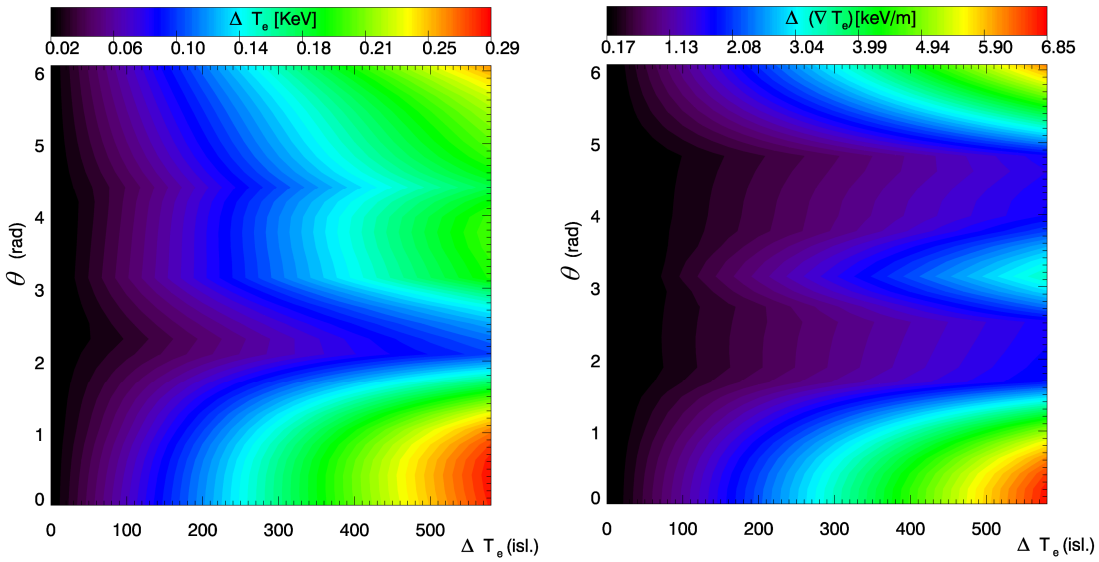

Fig1: left, maximum systematic deviation (relative value) of the measured DSXC T_e as a function of the QSH island phase and height; right, deviation in the value of ∇T_e.; gradients on the plot are much steeper when changing the island phase

The result of a sensitivity study is shown in Fig.1: the difference in the simulated profile and in the related temperature measure is plotted as a function of the T_e growth inside the island and of the island phase at the DSXC poloidal section. The major feature here is the dependence of the systematic errors on the island phase; this feature has to be accounted in the filtering of the datasets used in the gradient scaling analysis, in particular avoiding samples characterized by high phase dispersion.

3) Temperature gradient analysis and scaling

The T_e profile returned by the DSXC diagnostic gives informations on the highest value of the T_e gradient, which in turn is a good indicator of plasma confinement.

The ∇T_e value has been evaluated in three different ways: as the maximum slope between one point in the profile and the next one, and as the slope of two analytical fits, a 3rd degree polynomial (on 5-6 points in the ITB region) and a function in the form: $f(x) = A\left[1+\exp(x+B)\right]^{-1} + C$. These three indicators return in most cases similar values (Fig 2).

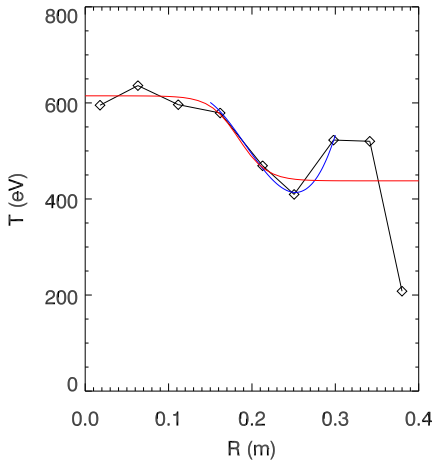

Fig 2:DSXC profile and fitting functions used in the analysis: red the exponential, blue the polinomial

The analysis has been performed on a database of over $2x10^5$ DSXC profiles coming from 159 shots with QSH cycles; for each QSH cycle, ∇T_e has been fitted as a function of the amplitude of dominant and secondary modes in the plasma, expecting a dependence in the form $|\nabla T| \propto A_{sec}^{\alpha} A_{dom}^{\beta}$; while the value of β does not differ significantly from zero [4], α show a Gaussian distribution (Fig. 3) peaked at -0.9 with σ~0.8.

Previous estimates [5] of the ∇T_e dependence on the amplitude of secondary modes in non-QSH shots returned exponent values around -1.4, which, given the dispersion in the samples, can be considered consistent with the value found here. However, a lower exponent can be referred to the minor importance of chaotic transport driven by magnetic turbulence in QSH with respect to non-QSH discharges.

A further step in the analysis is the study of variation in ITB position; also in this case, the sample has to be filtered accounting for the dominant mode phase, in order to discriminate only the structures intercepted by the DSXC fan in a correct way.

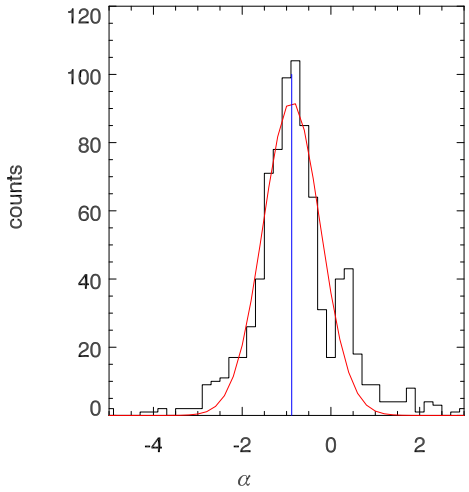

Fig 3: distribution of the α exponent ($\nabla T \propto A_{sec}^{\alpha} A_{dom}^{\beta}$)

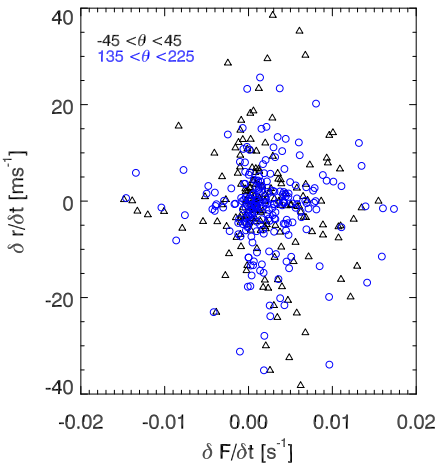

Fig 4: ITB velocities as a function of reversal parameter variation during the ramping phase of QSH cycles; there is nor a defined trend neither a preference for inward or

Nonetheless, there are no evidences of a movement of the flex point in the fitting function, expressed as a function of the time after the QSH cycle beginning or of the amplitude of dominant or secondary modes. As an example, Fig. 4 displays the time derivative of the barriers position as a function of the time derivative of reversal parameter F (which is related to the position of the external transport barrier). These results, in the limits of the DSXC spatial resolution, seem to indicate that, at the first order, the hot structure does not move but simply grows in temperature.

4) Electron diffusivity modeling and scaling.

The electron diffusivity has been evaluated via a simple 1-D power balance model; the diffusivity results here as $\chi_e = Q(n_e \nabla T_e)^{-1}$, where $Q = \int dr\left[P_\Omega(r) - \delta U(r)/\delta t\right]$ is the heat flux through the D-shaped magnetic surface surrounding the island; here P_Ω is the deposited ohmic power and U the plasma internal energy [6].

The scaling of χ_e as a function of secondary modes results in a slightly positive exponent, which does not vary in an appreciable way ($0.1<\alpha<0.4$) as the model parameters are changed (Fig 5). This result is quite different from the value of 2 expected from the Rechester-Rosenbluth approximation [7], which describes the transport rate in the hypothesis of complete magnetic stochasticity. Despite the high dispersion of the sample and the model approximations (especially in the P_Ω term evaluation), the difference is significant and suggests that, besides magnetic chaos, other contributions to the electron heat transport in the core can become important during QSH phases.

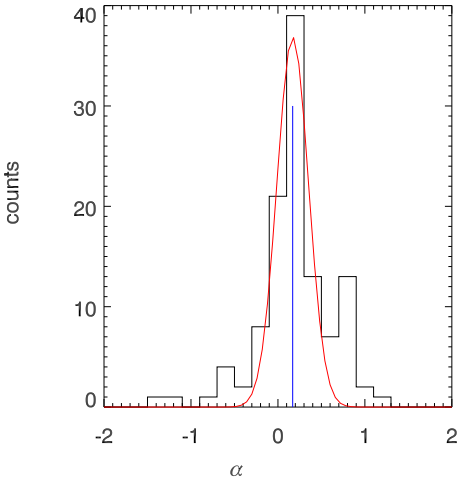

Fig 5: distribution of the α exponent in the electronic heat diffusivity scaling on secondary modes ($\chi_e \propto A_{sec}^{\alpha}$)

5) Final considerations and conclusions

On one side, the general dependence of the Te gradient on the magnetic chaos level is somehow confirmed, identifying a clear scaling exponent; on the other side, the absence of any systematic dependence in the ITB position on time, reversal parameter and magnetic spectrum suggests that, besides the tearing-like island growth toward a helical equilibrium (DAX-SHAx transition [8]), other phenomena can take place during a QSH early evolution.

The dependence of electron diffusivity on the magnetic spectra is somehow controversial, since it does not follow the expected trend; further analysis are ongoing.

6) References & Aknowledgement:

[1] Carraro L. *et al*., Nucl. Fusion **49**, 055009 (2009).
[2] Alfier A., Pasqualotto R., Rev. Sci. Instrum. **78**, 1 (2007).
[3] Bonomo F. et al., Rev. Sci. Instrum. **77,** 10F313 (2006).
[4] Innocente P. et al, Nucl. Fusion **47**, (2007).
[5] Frassinetti L. *et al*, Nucl. Fusion **48,** 045007 (2008).
[6] Fassina A. *et al*, EPS 2009 proc. P2-181, Sofia (2009).
[7] Rechester A.B., Rosenbluth M.N, Phys. Rev. Lett. **40**(38) (1978)
[8] Lorenzini R. *et al.*, Nature Physics **5**, 570 - 574 (2009).

This work was supported by the European Communities under the contract of Association between EURATOM/ENEA. The views and opinions expressed herein do not necessarily reflect those of European Commission